Journal of Global Positioning Systems (2025)
Vol. 21, Issue 1: 18-29
DOI:10.5081/jgps.21.1.18

Demystifying spatiotemporal relationship between GNSS-derived precipitable water vapor and ENSO index and its applications on floods and droughts

Yumeng Hao[1], Kefei Zhang[1,2,✉]

1 School of Environment Science and Spatial Informatics, China University of Mining and Technology, Xuzhou, 221116, China

2 College of Geodesy and Geomatics, Shandong University of Science and Technology, Qingdao, 266590, China

✉ Corresponding author, profkzhang@cumt.edu.cn

Abstract: The El Niño-Southern Oscillation (ENSO) is a complex ocean-atmosphere interaction phenomenon that drives extreme weather events globally, with water vapor playing a crucial role in its evolution. Recently, Global Navigation Satellite Systems (GNSSs) have emerged as an effective tool for retrieving water vapor with high accuracy, high spatial and temporal resolution, and all-weather capability. However, GNSS-derived precipitable water vapor (PWV) has not been well researched for its potential in the study of ENSO, particularly regarding their lead-lag relationships. This study investigates the spatiotemporal response relationship between PWV variations and the Oceanic Niño Index (ONI) using 12 years of coastal GNSS-derived PWV data. Multichannel singular spectrum analysis (MSSA) was employed to extract nonlinear trends of PWV anomalies, followed by Pearson correlation and lead-lag correlation analyses with ONI. The results reveal a moderate negative correlation in the western Pacific and positive correlations in the eastern Pacific and western Indian Ocean. Notably, stations closer to the Niño 3.4 region exhibited stronger correlations. Moreover, more than half of the stations showed absolute correlation coefficients exceeding 0.4 at optimal lag times, indicating that ENSO exerts a lagged influence on PWV at most stations. A case study at the COCO station near Indonesia (2015–2017) demonstrated that PWV and precipitation anomalies lagged ONI by approximately 8 months, consistent with the severe drought in 2015 and flooding in 2016. These findings suggest that GNSS-derived PWV serves as a valuable indicator for monitoring ENSO dynamics and could enhance early warning systems for ENSO-related drought and flood risks.

Keywords: GNSS-derived PWV; El Niño-Southern Oscillation; Oceanic Niño Index; Floods and droughts.

1 Introduction

The El Niño-Southern Oscillation (ENSO), driven by coupled ocean-atmosphere interactions, is a dominant mode of interannual climate variability, significantly influencing regional and global hydrometeorological patterns. ENSO events often lead to extreme weather phenomena, such as severe droughts and catastrophic floods, with substantial socio-economic and ecological consequences. Under the impact of global warming, both the frequency and intensity of ENSO events are expected to rise. For instance, Cai et al. predicted a twofold increase in extreme ENSO occurrences under future warming scenarios, highlighting the urgent need for systematic ENSO warning frameworks to better predict and manage associated risks [1]. However, a complete understanding of ENSO evolution and the accurate

prediction of its onset and impacts remain key challenges in climate science.

ENSO events are strongly influenced by their intensity, seasonal development timing, and interactions with other large-scale climate modes. For instance, during El Niño events, sea surface temperatures (SSTs) intensify ocean-atmosphere heat exchange and lead to increased evaporation rates and atmospheric water vapor content. The increased atmospheric water vapor, in turn, further amplifies SSTs, thereby reinforcing ENSO intensity. Consequently, predicting ENSO occurrence and impacts based solely on SST anomalies remains a persistent challenge. Additionally, ENSO signal strength is not always consistent with the magnitude of its hydrometeorological effects, such as total precipitation [2]. Therefore, integrating key atmospheric variables, particularly moisture transport and distribution metrics, is vital to advance the understanding and local-scale predictability of ENSO-induced impacts.

Precipitable water vapor (PWV) is one of the most dynamic components of the atmosphere, characterized by complex spatial distributions and rapid temporal variability. As PWV transport plays a critical role in the formation, evolution, and intensity of weather systems and is closely linked to extreme weather events [3], it serves as a key parameter in global climate change studies. Numerous studies have established relationships between climate change, PWV variations, and temperature (T) [4–6]. For example, Sun et al. demonstrated strong interannual correlations between tropical PWV and temperature variations, underscoring the significance of PWV in climate research [7]. Ground-based Global Navigation Satellite Systems (GNSSs) have become a leading technique for PWV monitoring, providing high accuracy, fine spatiotemporal resolution, cost-effectiveness, and all-weather reliability [3]. These advantages have made GNSS-derived PWV data invaluable for climate studies. Research by Wang et al. demonstrated that ENSO significantly influences GNSS-derived PWV variability, with a 1 K increase in SST corresponding to an 11% rise in PWV [4]. Similarly, Baidysz et al. observed distinct correlations between GNSS PWV anomalies and ENSO events, although these relationships exhibited regional and temporal variability [8]. Wang et al. used fast Fourier transform and wavelet transform methods to reveal the periodic variations in ZTD associated with ENSO [9]. To better quantify these connections, Zhao et al. developed an ENSO monitoring index based on GNSS PWV and temperature data [10]. However, this index did not account for the lag relationship between PWV and ENSO. Although these studies have provided valuable insights into PWV time series variations associated with ENSO, research on their lead-lag relationship and the prediction of droughts and floods influenced by ENSO remains limited. Therefore, this study aims to explore the lead-lag interactions between PWV and ENSO. By examining whether ENSO events precede or follow shifts in PWV time series, this research will enhance our understanding of their complex interactions. This will not only reveal the underlying impact patterns but also lay a foundation for improving ENSO prediction and better anticipating related extreme weather events.

In this study, PWV time series derived from 16 near-coastal International GNSS Service (IGS) stations between 2008 and 2019 were analyzed. The nonlinear trends of PWV anomalies were extracted using multichannel singular spectrum analysis (MSSA). The correlations and lead-lag relationships between the nonlinear trends of PWV and ENSO indices, such as the Oceanic Niño Index (ONI), were then analyzed. Additionally, the influence of ENSO events, specifically droughts and floods, on PWV variations at selected stations was investigated.

2 Datasets

2.1 GNSS-derived PWV

In this study, GNSS-derived ZTD data were obtained from the zenith path delay (ZPD) products provided by the IGS. As a global network comprising GNSS ground stations, data centers, and analysis centers, IGS delivers essential data and derived

products for Earth science research. The IGS ZPD products utilized in this work were generated by multiple analysis centers employing precise positioning techniques, featuring consistent formatting and high temporal resolution. Moreover, these products adhere to the unified IGS coordinate framework and stringent data quality standards, making them a reliable data source for high-precision water vapor estimation and spatiotemporal variation analysis. Figure 1 shows the spatial distribution of the 16 selected global GNSS stations (red triangles) and the two radiosonde stations (yellow pentagrams) used to validate the GNSS-derived PWV.

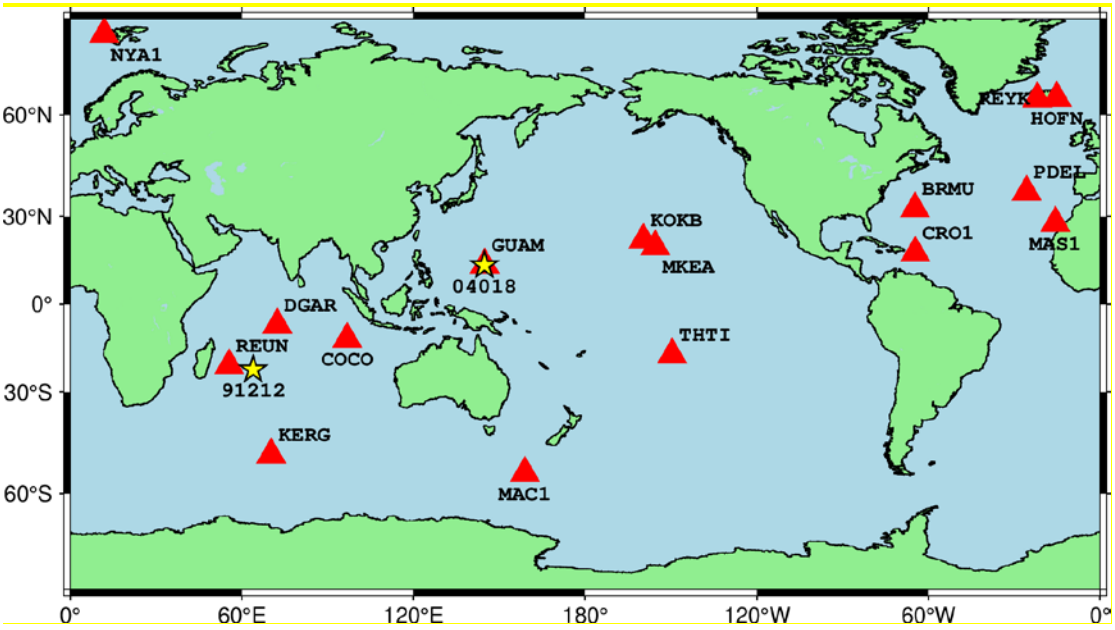

Figure 1. Spatial distribution of 16 GNSS stations (red triangles), 2 radiosonde stations (yellow pentagrams) across the globe.

Due to receiver malfunctions and/or poor observation conditions, missing data and outliers in ZTD time series are inevitable. Therefore, stations meeting the following criteria were selected: (1) a missing data rate <5%, (2) proximity to the sea (continental coasts or islands), and (3) a data gap period of less than one year. Based on these criteria, a total of 16 global IGS sites with valid data spanning the 12-year period from 2008 to 2019 were included in the study. To maintain a stable long-term time series for analysis, missing ZTD values were interpolated using the singular spectrum analysis for missing data (SSAM), while outliers were identified using the SSAM-IQR method (Interquartile Range) proposed by Wang et al. [11].

The conversion from ZTD to PWV can be achieved using the following formula:

$$PWV = \Pi \cdot ZWD = \Pi \cdot (ZTD - ZHD) \quad (1)$$

where *ZTD* is the zenith total delay value, *ZHD* is the zenith hydrostatic delay value, *ZWD* is the zenith wet delay value, and *Π* is a conversion factor.

$$ZHD = \frac{0.002277 \cdot P}{1 - 0.00266 \cdot \cos(2\varphi) - 0.00028 \cdot H} \quad (2)$$

where P refers to the surface pressure (in hPa), φ and H are the latitude and geodetic height in radians and kilometers, respectively.

$$\Pi = \frac{10^6}{\rho_w \cdot R_v \left[\frac{k_3}{T_m} + k_2'\right]} \quad (3)$$

where ρ_w is the water vapor density, R_v is the water vapor ratio constant with a value of $461.49\ J \cdot Kg^{-1} \cdot K^{-1}$, k_2' and k_3 are constants with values of $(22.1 \pm 2.2)\ K \cdot mb^{-1}$ and $(3.739 \pm 0.0012) \cdot 10^5\ K^2 \cdot mb^{-1}$, respectively [12]. T_m is the atmospheric weighted average temperature that is derived from the ERA5 temperature and humidity profiles, estimated as follows:

$$T_m = \frac{\int \frac{P_v}{T} d_z}{\int \frac{P_v}{T^2} d_z} \approx \frac{\sum_{i=1}^{N} \frac{P_{vi}}{T_i} \Delta Z_i}{\sum_{i=1}^{N} \frac{P_{vi}}{T_i^2} \Delta Z_i} \quad (4)$$

where P_v is the partial pressure (in hPa) of water vapor, T is the atmospheric temperature (in K), and i is the i-th pressure level. P_v can be calculated from

$$P_{si} = 6.11 \cdot 10^{\left(\frac{7.5 \cdot t_i}{237.3 + t_i}\right)} \quad (5)$$

$$P_{vi} = \frac{rh_i \cdot P_{si}}{100} \quad (6)$$

where P_s is the saturated vapor pressure, rh is relative humidity, and t is atmospheric temperature (in ℃).

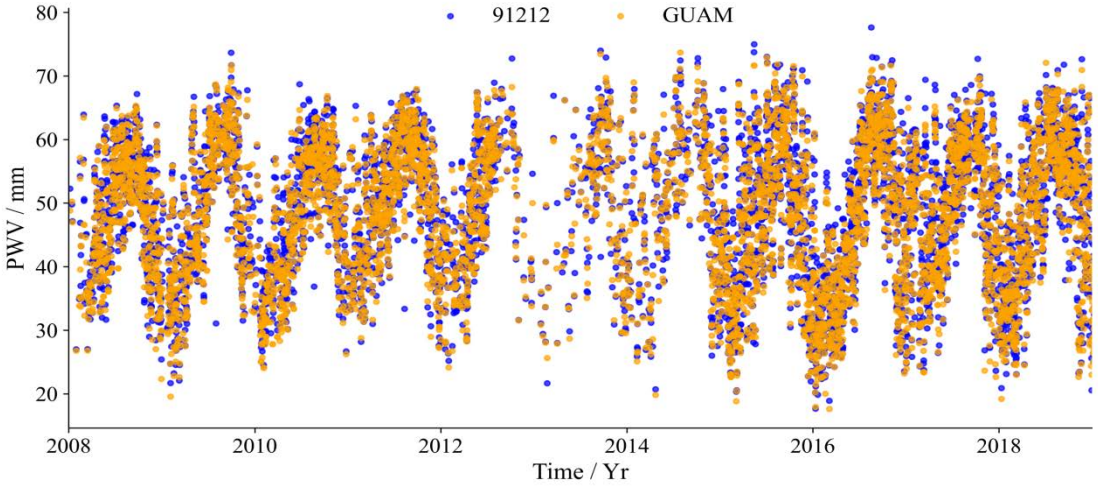

Figure 2. Comparison between radiosonde-derived PWV (91212 station) and GNSS-derived PWV (GUAM station).

To ensure the reliability and validity of the subsequent analyses, radiosonde data from the University of Wyoming Atmospheric Science Radiosonde Archive were employed to validate the accuracy of the GNSS-derived PWV. Specifically, radiosonde stations within 50 km horizontally and with an elevation difference of less than 200 m from the GNSS stations were selected as co-located validation sites [13]. These included stations 04018 and 91212. Reference PWV values were derived from integrated atmospheric profiles [14], achieving an accuracy better than 3 mm for GNSS-derived PWV, which meets operational standards for meteorological applications [4]. Figure 2 shows the comparison between radiosonde-derived PWV (91212 station) and GNSS-derived PWV (GUAM station). The data points for 2012–2014 appear sparser due to missing radiosonde-derived PWV observations at the 91212 station.

2.2 ERA5-provided SST, ZHD and Tm

ERA5, the fifth-generation ECMWF atmospheric reanalysis dataset, provides global climate data from January 1940 to the present. Specifically, it offers high-resolution coverage with a 31 km grid and 137 vertical levels, extending from the surface up to 80 km altitude. This dataset is generated by integrating observations with atmospheric models and data assimilation systems [15]. Therefore, the dataset is widely used in climate change studies [16] and short-term weather forecasting [17].

In this study, the ERA5 datasets gridded to a 2.5° × 2.5° resolution over a 12-year period were utilized. For SST, the ERA5 hourly data on single levels (1940–present) are employed, and subsequently interpolated to GNSS station locations using the inverse distance weighting (IDW) method.

Meanwhile, ZHD is calculated using the surface pressure, as described in Equation (2). However, due to the lack of pressure observations at the stations, ERA5 pressure values from the hourly data on pressure levels (1940–present) are used instead. Furthermore, the saturated vapor pressure, relative humidity, and atmospheric temperature required for calculating T_m are obtained from the ERA5 pressure-level product.

2.3 ONI and precipitation

To thoroughly investigate the relationship between variations of PWV and ENSO events, it is crucial to utilize climate indices that can precisely reflect both the strength and progression of ENSO phenomena. One of the most extensively used and authoritative indices for this purpose is the ONI. Specifically, ONI is obtained by the Climate Prediction Center (CPC) of the National Oceanic and Atmospheric Administration (NOAA) through continuous monitoring and statistical analysis of the SST anomalies in the east-central tropical Pacific. This area is known as the Niño 3.4 region (5°N–5°S, 120°W–170°W). According to the NOAA operational definition, an El Niño event is identified when the ONI remains at or above +0.5°C for five consecutive overlapping 3-month periods. Conversely, a La Niña event occurs when ONI values stay at or below –0.5°C for the same duration. When ONI values fluctuate between –0.5°C and +0.5°C, the conditions are generally considered ENSO-neutral [18]. Therefore, analyzing the relationship between the PWV and ONI time series can help reveal the influence of ENSO on atmospheric water vapor.

For other GNSS stations where in situ meteorological data on total precipitation were unavailable, monthly precipitation estimates from Version 2.3 of the Global Precipitation Climatology Project (GPCP) [19], a widely recognized global dataset, were utilized. The GPCP monthly precipitation data, provided on a 2.5°×2.5° grid, were interpolated to each GNSS station location using the IDW method.

3 Methodology

3.1 Multichannel singular spectrum analysis

Short-term extreme weather events—including typhoons, heavy rainfall, and flash droughts—can disrupt PWV time series. To mitigate their influence and more accurately isolate the impact of ENSO on PWV, MSSA was employed to extract the nonlinear trend from the PWV time series. MSSA is a non-parametric, data-adaptive method for time series decomposition and signal extraction, effectively separating a series into trend, oscillatory components (e.g., seasonal or quasi-periodic signals), and noise without requiring a priori assumptions about underlying physical processes [20]. This makes it particularly well-suited for analyzing complex atmospheric variables like PWV, which are often influenced by overlapping signals and noise.

Given that the ONI is derived from monthly sea surface temperature (SST) anomalies, its temporal resolution corresponds to monthly scales. To maintain consistency, monthly PWV averages were first computed over the 12-year study period, and PWV anomalies were derived by subtracting the corresponding monthly means. The baseline was defined as the mean PWV value for each corresponding month over the 12-year study period. For example, the baseline for January was calculated as the mean PWV of all January values within the study period. MSSA was then applied to the PWV anomaly series (window length = 12), and the first eight eigencomponents were reconstructed and combined to obtain the dominant nonlinear trend. This reconstructed trend was then correlated with the ONI time series using Pearson and lead–lag correlation analyses.

3.2 Pearson correlation analysis

The relationship between GNSS-derived PWV time series and the ONI is examined using Pearson correlation analysis. This is a widely used statistical method for quantifying linear associations between continuous variables. The Pearson correlation coefficient, which ranges from –1 to +1, quantifies

both the strength and direction of the relationship between two variables. Positive values indicate a direct correlation, whereas negative values signify an inverse correlation. The closer the coefficient is to ±1, the stronger the association between the variables [21]. This analysis provides a preliminary assessment of the statistical linkage between PWV fluctuations and ENSO intensity, offering insights into how ENSO influences GNSS-derived PWV variability.

3.3 Lead-lag correlation analysis

Lead-lag correlation analysis was conducted to explore the temporal dependency between PWV and ONI. Lead-lag correlation is a statistical technique used to determine whether variations in one time series precede (lead) or follow (lag) those in another [22]. In this study, the nonlinear GNSS-derived PWV time series and ONI values were compared over a range of time lags, typically from several months before to several months after ENSO peaks, in order to capture the full dynamic interaction. By shifting the ONI time series backward and forward relative to the PWV series and computing Pearson correlation coefficients at each lag step, this method revealed the time delay or advance at which the association between the two variables is strongest. Positive lags indicate that changes in ONI precede changes in PWV, while negative lags suggest that PWV responds prior to ENSO signals. This enables the responses of atmospheric water vapor on ENSO events.

4 Results and discussion

To analyze the variation of GNSS-derived PWV under the influence of ENSO, the correlation between the ONI time series and the nonlinear trend of PWV anomalies was calculated. Figure 3 presents the correlation coefficients between the ONI time series and the nonlinear trends of PWV anomalies at GNSS stations.

The results reveal a moderate negative correlation in the western Pacific region, particularly at GUAM and MAC1, indicating that PWV tends to decrease during El Niño events (when ONI increases), potentially elevating drought risks in this region. In contrast, a moderate positive correlation is observed in the eastern Pacific, notably at stations KOKB, MKEA, and THTI, with THTI showing the strongest correlation (0.60). This is likely because THTI is geographically closest to the Niño 3.4 region, where the ONI index is calculated. These findings suggest that PWV in the eastern Pacific tends to increase during El Niño periods, potentially resulting in enhanced precipitation. In the Indian Ocean region, stations such as DGAR, REUN, and KERG exhibit a positive correlation between the PWV anomalies trend and the ONI time series. This indicates that PWV increases during El Niño and decreases during La Niña, which is consistent with the conclusions of [23].

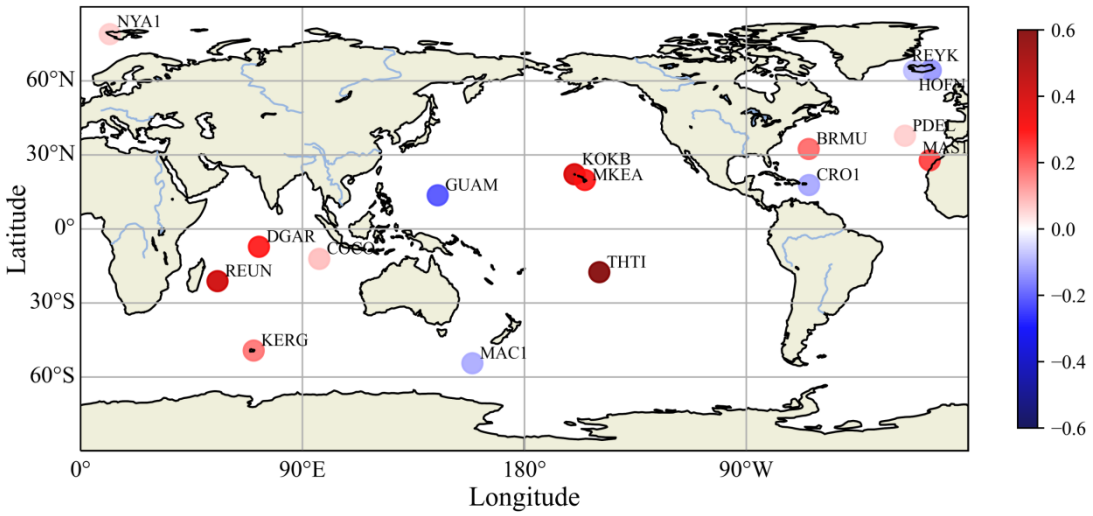

Figure 3. Spatial distribution of the correlation coefficients between ONI time series and nonlinear trend of PWV anomalies at GNSS stations.

Additionally, MAS1, located in the eastern Atlantic near North Africa, and BRMU, situated in the Bermuda region, both show positive correlations. Conversely, CRO1, located in the Caribbean, shows a negative correlation. This divergence may be partly explained by distinct large-scale teleconnection pathways influencing each region. Specifically, the Caribbean may be more directly affected by enhanced cold air advection and subsidence associated with La Niña, which could lead to cooler and drier conditions. In contrast, Bermuda, positioned at a higher latitude, appears to be influenced by the Pacific-North American (PNA) pattern and related Atlantic teleconnections that tend to intensify during El Niño events. These circulation anomalies may promote warm and moist air advection from lower latitudes, thereby contributing to the positive PWV-ONI correlations observed at BRMU [24–26]. Finally, stations such as NYA1, REYK, and HOFN show weak correlations, likely due to their high-latitude positions (above 60°N) and substantial distance from the ENSO source regions, which reduces their sensitivity to ENSO-related atmospheric signals.

Table 1. The best lags and the correlation coefficients at that lag for the relationship between ONI time series and the nonlinear trend of PWV anomalies at GNSS stations.

Station name	Best lag (months)	Correlation coefficient	Station name	Best lag (months)	Correlation coefficient
BRMU	11	0.48	MAC1	0	–0.09
GUAM	4	–0.59	MKEA	–8	0.29
KERG	7	0.22	MAS1	–1	0.23
KOKB	–11	0.57	NYA1	3	–0.03
COCO	8	0.68	PDEL	–8	0.05
CRO1	–5	–0.31	REYK	8	0.48
DGAR	3	0.41	REUN	–1	0.42
HOFN	10	0.30	THTI	4	0.67

To further investigate the response mechanism of PWV to ENSO, we computed the lagged and lead correlations between the ONI time series and the nonlinear trends of PWV anomalies. Figure 4 shows the spatial distribution of the best lag between ONI time series and the nonlinear trends of PWV anomalies at GNSS stations, while Table 1 lists the best lags and the corresponding correlation coefficients at those lags for each station. A negative best lag indicates that the PWV time series leads the ONI time series, suggesting that PWV could serve as a precursor signal for ENSO development. Conversely, a positive best lag suggests that PWV responds to ENSO with a delay.

According to Table 1, nine stations (56.3%) exhibit absolute correlation coefficients greater than 0.4 at their respective best lags, indicating a moderately strong ENSO-PWV relationship. At MAC1, no significant lag was found between the ONI time series and the nonlinear trend of PWV anomalies, suggesting that changes in PWV occur simultaneously with ENSO events. In contrast, at NYA1 and PDEL, the correlation coefficients at the best lags are close to zero and comparable to their Pearson correlation values, implying that their best lags are not meaningful in a physical sense.

As illustrated in Figure 4, stations KOKB, MKEA, and REUN exhibit negative best lags, indicating that PWV changes precede ENSO signals at these locations. Specifically, the negative correlation observed at KOKB and MKEA may be related to the influence of the North Pacific

Subtropical Gyre (NPSG), a large-scale clockwise oceanic circulation system that transports water from the northeastern Pacific to the Hawaiian region. Depending on the velocity of this current system, the time required for relatively cool high-latitude waters to reach the subtropics varies. Slower transport allows more time for sea surface warming en route, potentially leading to higher PWV anomalies, while faster transport reduces this warming period, resulting in lower anomalies [8]. This interpretation should be regarded as a plausible hypothesis, with further validation using oceanic circulation data warranted in future work.

These findings provide valuable insights into the spatiotemporal variability of PWV responses to ENSO, and help establish a more nuanced propagation mechanism model of ENSO-related atmospheric and oceanic interactions.

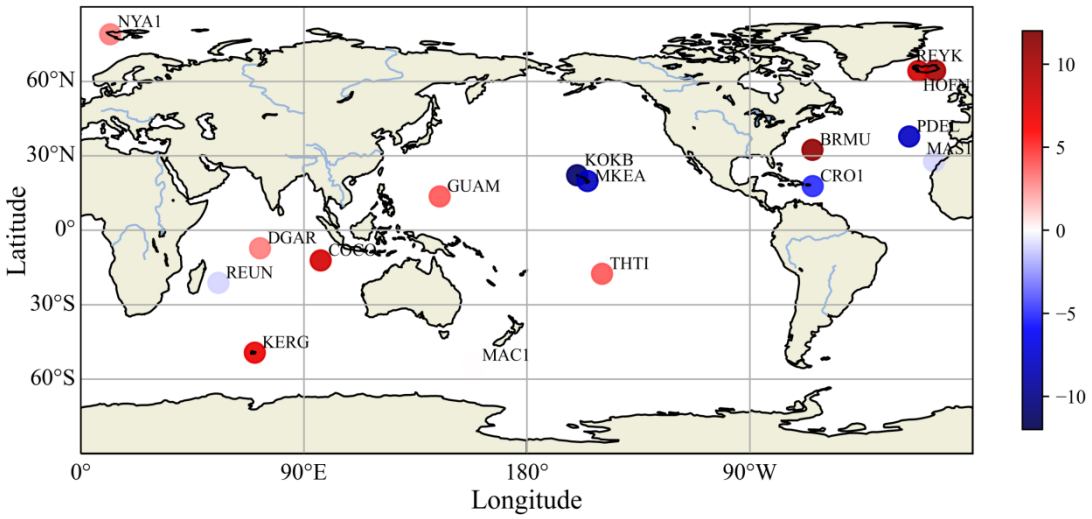

Figure 4. Spatial distribution of the best lag between ONI time series and the nonlinear trend of PWV anomalies at GNSS stations.

To provide a more intuitive demonstration of the above analysis results, a representative case was selected, and precipitation anomalies were incorporated as an additional variable for analysis. The precipitation anomalies were calculated as deviations from their respective monthly baselines, which were defined as the mean precipitation for each corresponding month over the 12-year study period (e.g., the January baseline corresponds to the average precipitation of all January values during the study period). Figure 5 illustrates the nonlinear trend of PWV anomalies, precipitation anomalies, and the ONI time series at the COCO station, located near Indonesia. The results reveal that PWV and precipitation anomalies exhibit highly synchronous variations, both reaching their lowest values in June 2015, followed by a steady increase, and peaking in April 2016. During this period, positive PWV values were observed from December 2015 to October 2016, whereas positive ONI values occurred from April 2015 to April 2016, indicating a lag of approximately 8 months in PWV response relative to ONI. This finding is consistent with the results of the lead-lag correlation analysis discussed earlier.

Furthermore, according to a report released by the National Institute of Aeronautics and Space of Indonesia, the country experienced its most severe drought in nearly two decades in 2015 [27]. In April 2016, Sumatra Island was hit by severe flooding and landslides [28]. These observations further support the notion that extreme positive or negative ONI values can trigger both drought and flood events. Therefore, this suggests that analyzing the lag relationship between PWV and the ONI time series can serve as a scientific basis for early warning of regional droughts and floods,

and contribute to a better understanding of the disaster response mechanisms of atmospheric water vapor under ENSO influences.

5 Conclusions

An in-depth understanding of water vapor variability is essential for studying various climate phenomena such as ENSO. However, current knowledge of PWV time series variations under ENSO influence remains limited, particularly regarding their lead-lag relationship. Over the past three decades, GNSS technology has enabled accurate PWV estimation, providing a valuable dataset for capturing highly dynamic atmospheric moisture variations. GNSS-derived PWV data from 16 coastal stations over a 12-year period were used to investigate the relationship between PWV and ONI—a widely used ENSO indicator. The MSSA method extracted the nonlinear trend of PWV anomalies, which was then analyzed using Pearson and lead-lag correlation techniques with respect to ONI. The results reveal moderate negative correlations in the western Pacific, moderate positive correlations in the eastern Pacific, and positive correlations in the western Indian Ocean. Stations closer to the Niño 3.4 region (where ONI is defined) exhibit stronger correlations, while those farther away show weaker associations. Notably, more than half of the stations (9 out of 16) display absolute correlation coefficients exceeding 0.4 at their optimal lags, indicating a moderately strong ENSO-PWV relationship. Additionally, four stations exhibit PWV responses preceding ONI, potentially linked to statistical artifacts or other climatic factors.

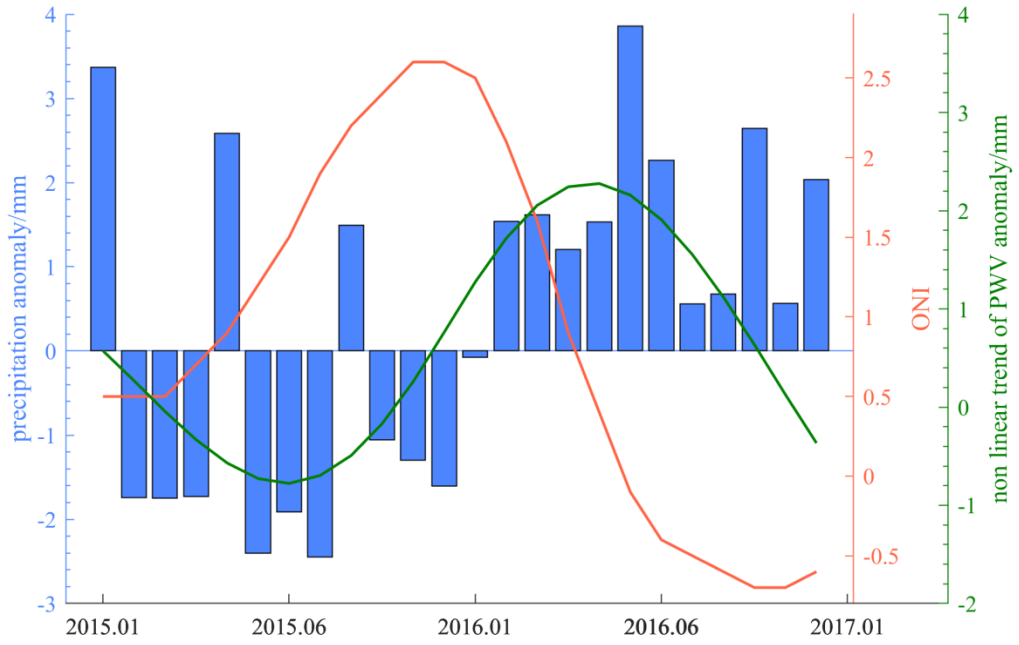

Figure 5. The nonlinear trend of PWV anomalies, ONI time series and precipitation anomalies at COCO during 2015−2017

As a coupled ocean–atmosphere phenomenon, ENSO significantly influences atmospheric water vapor content, often triggering hydrometeorological extremes such as floods and droughts. Monitoring GNSS-derived PWV variations thus offers a promising approach for studying ENSO impacts. A case study using data from the COCO station near Indonesia (2015–2017) supports this conclusion: PWV and precipitation showed highly synchronized variability, both lagging ONI by approximately 8 months, coinciding with observed droughts in 2015 and floods/landslides in 2016. These findings suggest that ENSO events can substantially modulate the temporal evolution of PWV at specific stations.

Overall, this study underscores the utility of GNSS-derived PWV for improving our understanding of atmospheric water vapor responses to ENSO and highlights its potential for monitoring and anticipating ENSO-related hydrometeorological anomalies.

Reference

[1] Cai, W., Guilyardi, E., Vecchi, G., England, M. H., Wang, G., Collins, M., Lengaigne, M., Borlace, S., Mcphaden, M. J., Wu, L., Timmermann, A., Santoso, A., Jin, F.-F., & Van Rensch, P. (2014). Increasing frequency of extreme El Niño events due to greenhouse warming. Nature Climate Change, 4(2), 111–116. doi.org/10.1038/nclimate2100.

[2] Wang, S., Li, Y., & Yuan, X. (2017). Does a Strong El Niño Imply a Higher Predictability of Extreme Drought? Scientific Reports, 7(1). doi.org/10.1038/srep40741.

[3] Vaquero-Martínez, J., & Antón, M. (2021). Review on the Role of GNSS Meteorology in Monitoring Water Vapor for Atmospheric Physics. Remote Sensing, 13(12), 2287. doi.org/10.3390/rs13122287.

[4] Wang, X., Zhang, K., Wu, S., Li, Z., Cheng, Y., Li, L., & Yuan, H. (2018). The correlation between GNSS-derived precipitable water vapor and sea surface temperature and its responses to El Niño–Southern Oscillation. Remote Sensing of Environment, 216, 1–12. doi.org/10.1016/j.rse.2018.06.029.

[5] Trenberth, K. E., Dai, A., Rasmussen, R. M., & Parsons, D. B. (2003). The Changing Character of Precipitation. Bulletin of the American Meteorological Society, 84(9), 1205–1218. doi.org/10.1175/bams-84-9-1205.

[6] Alshawaf, F., Wickert, J., Balidakis, K., Dick, G., & Heise, S. (2017). Estimating trends in atmospheric water vapor and temperature time series over Germany. Atmospheric Measurement Techniques, 10(9), 3117–3132. doi.org/10.5194/amt-10-3117-2017.

[7] Sun, D. Z., & Held, I. M. (1996). A comparison of modeled and observed relationships between interannual variations of water vapor and temperature. Journal of Climate, 9(4), 665–675. doi.org/10.1175/1520-0442(1996)0092.0.co;2.

[8] Baldysz, Z., Baranowski, D. B., Figurski, M., Latos, B., & Nykiel, G. (2021). Interannual Variability of the GNSS Precipitable Water Vapor in the Global Tropics. Atmosphere, 12(12), 1698. https://doi.org/10.3390/atmos12121698.

[9] Wang, Y., Yu, T., Liu, X., & Zhan, W. (2021). GNSS ZTD time series in Beijing-Tianjin-Hebei region and their response to El Niño events. Journal of Nanjing University of Information Science & Technology, 13(2), 170–180.

[10] Zhao, Q., Ma, X., Yao, W., Liu, Y., & Yao, Y. (2020). A Novel ENSO Monitoring Method using Precipitable Water Vapor and Temperature in Southeast China. Remote Sensing, 12(4), 649. doi.org/10.3390/rs12040649.

[11] Wang, X., Cheng, Y., Wu, S., & Zhang, K. (2016). An effective toolkit for the interpolation and gross error detection of GPS time series. Survey Review, 48(348), 202–211. doi.org/10.1179/1752270615y.0000000023.

[12] Bevis, M., Herring, T. A., Ware, R. H., Businger, S., Rocken, C., & Anthes, R. A. (1992). GPS meteorology: Remote sensing of atmospheric water vapor using the global positioning system. Journal of Geophysical Research: Atmospheres, 97(D14), 15787–15801. doi.org/10.1029/92jd01517.

[13] Zhang, W., Lou, Y., Haase, J. S., Zhang, R., Zheng, G., Huang, J., Shi, C., & Liu, J. (2017). The Use of Ground-Based GPS Precipitable Water Measurements over China to Assess Radiosonde and ERA-Interim Moisture Trends and Errors from 1999 to 2015. Journal of Climate, 30(19), 7643–7667. doi.org/10.1175/jcli-d-16-0591.1.

[14] Zhang, Q., Zhang, S., Han, F., & Ye, J. (2018). Precipitable Water Vapor Retrieval and Analysis

by Multiple Data Sources: Ground-Based GNSS, Radio Occultation, Radiosonde, Microwave Satellite, and NWP Reanalysis Data. Journal of Sensors, 2018, 1–13. doi.org/10.1155/2018/3428303.

[15] Palmer, T. N., Petroliagis, T., Buizza, R., & Barkmeijer, J. (1997). The ECMWF Ensemble Prediction System. Meteorological Applications, 4(4), 301–304. doi.org/10.1017/s1350482797000649.

[16] Jung, T., Altshuler, E. L., Palmer, T. N., Wedi, N., Miller, M. J., Marx, L., Achuthavarier, D., Hodges, K. I., Cash, B. A., Stan, C., Towers, P., Kinter, J. L., & Adams, J. M. (2012). High-Resolution Global Climate Simulations with the ECMWF Model in Project Athena: Experimental Design, Model Climate, and Seasonal Forecast Skill. Journal of Climate, 25(9), 3155–3172. doi.org/10.1175/jcli-d-11-00265.1.

[17] Verkade, J. S., Brown, J. D., Reggiani, P., & Weerts, A. H. (2013). Post-processing ECMWF precipitation and temperature ensemble reforecasts for operational hydrologic forecasting at various spatial scales. Journal of Hydrology, 501, 73–91. doi.org/10.1016/j.jhydrol.2013.07.039.

[18] Chen, Z., Li, J., Luo, J., & Cao, X. (2018). A New Strategy for Extracting ENSO Related Signals in the Troposphere and Lower Stratosphere from GNSS RO Specific Humidity Observations. Remote Sensing, 10(4), 503. doi.org/10.3390/rs10040503.

[19] Adler, R. F., Schneider, U., Janowiak, J., Susskind, J., Huffman, G. J., Nelkin, E., Arkin, P., Xie, P.-P., Rudolf, B., Chang, A., Ferraro, R., Gruber, A., Bolvin, D., & Curtis, S. (2003). The Version-2 Global Precipitation Climatology Project (GPCP) Monthly Precipitation Analysis (1979–Present). Journal of Hydrometeorology, 4(6), 1147–1167. doi.org/10.1175/1525-7541(2003)0042.0.co;2.

[20] Vautard, R., Yiou, P., & Ghil, M. (1992). Singular-spectrum analysis: A toolkit for short, noisy chaotic signals. Physica D: Nonlinear Phenomena, 58(1–4), 95–126. doi.org/10.1016/0167-2789(92)90103-t.

[21] Guo, M., Xia, P., & Zhang, H. (2021). Exploration and analysis of the factors influencing GNSS PWV for nowcasting applications. Advances in Space Research, 67(12), 3960–3978. doi.org/10.1016/j.asr.2021.02.018.

[22] Yim, S.-Y., Xing, W., & Wang, B. (2015). Peak-summer East Asian rainfall predictability and prediction part II: extratropical East Asia. Climate Dynamics, 47(1–2), 15–30. doi.org/10.1007/s00382-015-2849-x.

[23] Suparta, W., Gaol, F. L., & Iskandar, A. (2017). GPS PWV and Its Response to ENSO Activities in the Western Pacific Region During 2009–2011 (pp. 157–172). springer Singapore. doi.org/10.1007/978-981-10-6574-3_14.

[24] Jury, M. R., & Enfield, D. B. (2010). Environmental Patterns Associated with Active and Inactive Caribbean Hurricane Seasons. Journal of Climate, 23(8), 2146–2160. doi.org/10.1175/2009jcli3201.1.

[25] Chiang, J. C. H., & Lintner, B. R. (2005). Mechanisms of Remote Tropical Surface Warming during El Niño. Journal of Climate, 18(20), 4130–4149. doi.org/10.1175/jcli3529.1.

[26] Lee, S., Wang, C., & Enfield, D. B. (2008). Why do some El Niños have no impact on tropical North Atlantic SST? Geophysical Research Letters, 35(16). doi.org/10.1029/2008gl034734.

[27] Lestari, D. O., Sabaruddin, S., Iskandar, I., & Sutriyono, E. (2018). Severe Drought Event in Indonesia Following 2015/16 El Niño/positive Indian Dipole Events. Journal of Physics: Conference Series, 1011(1), 012040. doi.org/10.1088/1742-6596/1011/1/012040.

[28] United Nations Office for the Coordination of Humanitarian Affairs. (2016). *Indonesia: April 2016 - Humanitarian snapshot (Report No. 3).

Authors

Yumeng Hao received her B.Sc. in the School of Environment Science and Spatial Informatics, China University of Mining and Technology, Xuzhou, China, in 2022. She is currently pursuing a Ph.D. in the School of Environment Science and Spatial Informatics, China University of Mining and Technology, Xuzhou, China. Her main research interests include GNSS Meteorology.

Kefei Zhang is currently a distinguished professor and Director of the Institute of Resources and Environment Technologies at China University of Mining and Technology (CUMT), China. He is also an honorary professor of RMIT University in Australia where he is the Founding Director of the Satellite Positioning for Atmosphere, Climate and Environment (SPACE) Research Centre. Professor Zhang has received his Ph.D. from Curtin University, Australia in 1998 and is also a Fellow of The International Association of Geodesy (IAG). He has over 30 years of research experience in geodesy, satellite positioning and geospatial sciences in general. He has authored about 500 peer-reviewed publications in these fields and a co-inventor of thirty patents, and attracted significant amount of research funding from the Australian Research Council, the National Science Foundation of China, as well as funds from other national and international organization and industries. Professor Zhang is an Australian pioneer in cutting-edge technological applications for smart tracking, GNSS atmospheric sounding for weather and climate, and space resources exploitation and exploration etc. His satellite tracking frontier research has contributed to 10-h weather forecast improvement and successful integration of the GPS radio occultation data into the Australian weather forecasting system in 2012. His current research interests lie primarily in algorithm development and innovative applications of satellite technologies for high accuracy positioning, atmospheric sounding, space situational awareness, and space resources utilization. He currently leads a team of over 50 researchers at CUMT.